Efficient Coupling of Reaction Pathways of Criegee Intermediates and Free Radicals in the Heterogeneous Ozonolysis of Alkenes

Meirong Zeng and Kevin R. Wilson*

Chemical Sciences Division, Lawrence Berkeley National Laboratory, Berkeley, CA 94720, USA.

KEYWORDS. unsaturated alkene aerosols, Criegee intermediates, ozone chemistry, heterogeneous reactions, multiphase chemistry, free radicals

ABSTRACT: In the gas-phase, ozonolysis of olefins is known to be a significant source of free radicals. However, for heterogeneous and condensed phase ozone reactions the importance of reaction pathways that couple Criegee intermediates (CI) with hydroxyl (OH), alkoxy, and peroxy free radicals remains uncertain. Here we report experimental evidence for substantial free radical oxidation during the heterogeneous reaction of O_3 with cis-9-tricosene (Tri) aerosol. A kinetic model with three coupled sub-mechanisms that include O_3, CI, and free radical reactions is used to explain how the observed Tri reactivity and its product distributions depend upon [O_3], [OH], and the presence of CI scavengers. During multiphase ozonolysis, the kinetic model predicts that only ~ 30% of the alkene is actually consumed by O_3, while the remaining ~ 70% is consumed by free radicals that cycle through pathways involving CI. These results reveal the importance of free radical oxidation during heterogeneous ozonolysis, which has been previously difficult to isolate due to the complex coupling of CI and OH reaction pathways.

In the environment, multiphase oxidation of organic molecules play a central role in air pollution and aerosol formation chemistry, which in turn have larger scale impacts on human health and climate.[1-4] The two most important oxidants are ozone (O_3) and the hydroxyl radical (OH) that together account for the majority of oxidative transformations in the troposphere.[5] Oxidation proceeds through networks of many elementary reactions involving highly reactive intermediates.[3,6] With a few exceptions, O_3 and OH reactions proceed by separate mechanisms involving distinct intermediates. O_3 reactions produce Criegee intermediates (CI),[7-9] while OH oxidation proceeds through elementary reactions of peroxy and alkoxy free radicals.[6] Here we examine the heterogeneous ozonolysis of a model alkene and find evidence that oxidation proceed by the substantial coupling between reaction pathways of CI and peroxy/alkoxy radicals.

In the gas phase, O_3 reacts with alkenes to produce CI that decompose to produce OH [10-13] and a vinoxy radical (RO) co-product in substantial yields (e.g. 0.3 for cis-3-hexene[10]). This is one of the main mechanistic links between free radical oxidation and ozonolysis. In contrast, the importance of OH production during heterogeneous reactions of O_3 with alkene surfaces (i.e. aerosol) remains more uncertain,[14-19] in part because previous studies have not universally observed oxidation products that could be unambiguously attributed to OH. This is likely explained by recent results reported by Beauchamp and coworkers,[20,21] who observed evidence for a new reaction pathway where β-hydroxy-peroxy radicals (β-RO_2), formed in the presence of O_2 when OH adds to a C=C bond, undergo facile bond scission to produce CI.[20,21] The β-RO_2 intermediate connects ozonolysis and free radical oxidation pathways in a new way that was later implicated in chain cycling mechanisms (i.e. OH → β-RO_2 → CI → OH) in the autoxidation of unsaturated lipids.[22] The β-RO_2 → CI pathway suggests that definitive observations of OH reaction products in previous studies is likely difficult,[14,15,23] since O_3 and OH could form similar products (i.e. secondary ozonides, aldehydes). Here we report experimental results and kinetic modeling that reveals the importance of free radical generation in multiphase ozonolysis, which contributes substantially to the overall oxidation rate of an unsaturated aerosol.

A flow reactor[15] (*see Section S1 and Fig. S1 of Supporting information*) is used to investigate the heterogeneous reactions of O_3 with a model organic aerosol comprised of cis-9-tricosene (Tri, $C_{23}H_{46}$, as shown in Fig. 1A). Tri is selected as a model system since it has a simple molecular structure, a single C=C bond and multiple C-H sites (6 primary, 34 secondary, 2 vinylic, and 4 secondary allylic C-H sites) for H-abstraction by OH. Importantly, this molecule lacks oxygen functional groups (e.g. carbonyls or acids) that undergo bimolecular reactions with CI, which simplifies product assignments and enhances our ability to observe evidence for unimolecular decomposition of the CI. To separate pathways due solely to OH reactions from those involving ozonolysis, an additional set of experiments (without O_3) were conducted in a continuous flow tank reactor (CFSTR) as shown in Fig. S2.[22,24] For both reactors, kinetics and products are measured in real time using a vacuum ultraviolet aerosol mass spectrometer (VUV-AMS).[25]

Previous OH oxidation studies of organic aerosols, comprised of chemically reduced, saturated organic molecules (i.e. hydrocarbons), identified major oxidation products as ketones and alcohols.[6,24,26-28] These oxygen functional groups form via H-abstraction by OH, followed by O_2 addition to the resulting alkyl radical, to form peroxy radicals (RO_2). In the absence of HO_2, RO_2 reacts with other RO_2 to form ketones and alcohols by the well-known Russell and/or Bennett Summers mechanisms.[29-32] The net reaction replaces a C-H group with either a C-OH or C=O moiety. In a liquid aerosol, repeated OH attack occurs sequentially and forms multiple generations of oxygenated products with a Poisson distribution of ketone/alcohol functional groups.[28]

Shown in Fig. 1A is a mass spectrum of the oxidation products observed in the Tri + OH reaction. Products denoted as TriO and $TriO_2$ (molecular structures illustrated in Fig. 1B) are consistent with the previous H-abstraction mechanism discussed above. Additional peaks in the mass spectra appear at m/z = 212 and 228 and correspond to $C_{14}H_{28}O$ and $C_{14}H_{28}O_2$, respectively. $C_{14}H_{28}O$ is assigned to n-tetradecanal, which is formed by pathways shown in Fig. S3. $C_{14}H_{28}O_2$ could be a fragment (or a product) of the C_{14} α-hydroxyalkyl hydroperoxide (C_{14} HAH, m/z = 246) as shown in Fig. S4. The TriO and $TriO_2$ products are different from those formed by ozone reactions, which are lower molecular weight aldehydes, produced when the primary ozonide (POZ) decomposes, and secondary ozonides (SOZs) formed by the reaction of a CI with a carbonyl.[15,23,33] So in this system, TriO and $TriO_2$ serve as fingerprints for the presence of OH chemistry.

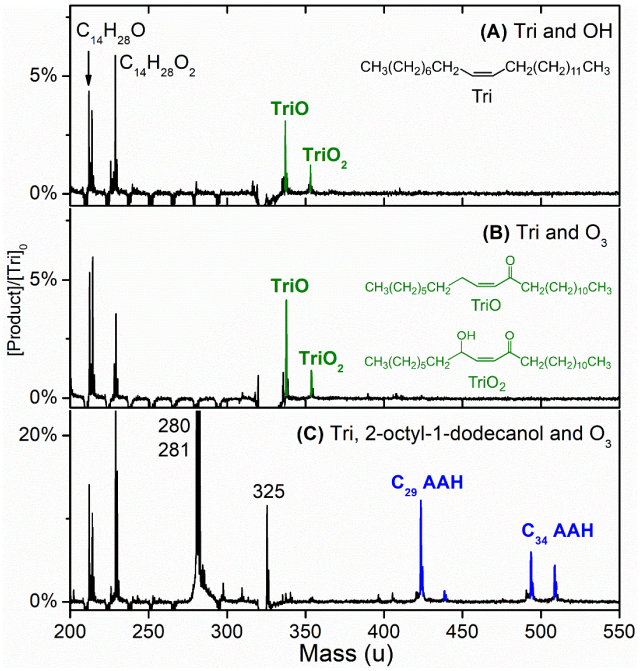

Figure 1. Difference mass spectra (unreacted Tri – reacted Tri) shows major reaction products of cis-9-tricosene (Tri), such as ketone (TriO and $TriO_2$) and α-alkoxyalkyl hydroperoxide (AHH). (A) Reaction products during the Tri + OH reactions in the CFSTR ([OH] ~ 1.6×10^7 molecules·cm^{-3}). (B and C) Reaction products observed during the Tri + O_3 reactions without (B) and with the 2-octyl-1-dodecanol (C) ([O_3] ~ 4.0×10^{13} molecules·cm^{-3}). The chemical structures of Tri and possible isomers of TriO and $TriO_2$ are shown as insets. Structures of the C_{29} and C_{34} AAH are shown in Fig. S3.

As shown in Fig. 1B, the same TriO and $TriO_2$ products appear in the Tri + O_3 reactions. SOZ products, typical of ozonolysis in other systems,[15,23,34] are not detected. This is due to the location of the C=C bond in Tri, which during bond scission of the POZ, produces a volatile C_9 and semi-volatile C_{14} aldehyde (m/z = 212, Fig. 1), as shown in Fig. S3. A substantial fraction (c.a. >80%) of the C_9 and C_{14} aldehydes partition to the gas phase[35] and explains why SOZs are not observed in this system as discussed in Ref.[22] and Sections S1.2 and S2.1. The observation of TriO and $TriO_2$ products in separate O_3 and OH experiments provides evidence for the production of OH during ozonolysis; likely formed by unimolecular scission of the CI to form OH and an alkoxy (RO) radical co-product as is well known in gas phase.[36,37]

A CI scavenger (a saturated liquid alcohol, 2-octyl-1-dodecanol) is added to the aerosol prior to ozonolysis. Although unreactive towards O_3, 2-octyl-1-dodecanol reacts efficiently with CI to produce a distinctive α-alkoxyalkyl hydroperoxide (AAH) products[38,39] as shown in Fig. 1C. With the addition of the scavenger, the peaks corresponding to TriO and $TriO_2$ disappear, instead yielding new peaks in the mass spectrum located between m/z = 400 and 550. These peaks are assigned to AAHs, once fragmentation (likely due to dissociative photoionization) is considered as shown in Figs. S3 and S5 and discussed in Ref.[22]. These observations point to a mechanistic link between the CI and the formation pathways of TriO and $TriO_2$.

To quantify the significance of these free radical reaction pathways in ozonolysis, Tri reaction probabilities (or effective uptake coefficients, γ_{eff}) are quantified as a function of the amount of the CI scavenger (i.e. 2-octyl-1-dodecanol) in the aerosol phase, as shown in Fig. 2A. γ_{eff} is the fraction of surface ozone collisions with Tri that yield a reaction as described previously.[26,40] Without the CI scavenger, γ_{eff} for Tri is determined to be 5.2×10^{-4}. This value is larger than previous measurements (6×10^{-5})[41] that quantified uptake by the loss of O_3 above a Tri surface. This difference in uptake coefficient is expected since gas phase determinations of reactive uptake are insensitive to secondary radical chemistry occurring in the particle-phase.[41]

If O_3 were the only species to react with Tri, then γ_{eff} would remain unchanged with alcohol fraction, since γ_{eff} is normalized to the quantity of Tri in the aerosol. Instead, γ_{eff} decreases by ~ 2x indicating that increasing the alcohol fraction removes a substantial second reactive sink for Tri (Fig. 2A). This is accompanied by a decrease in TriO and, as expected, the AAHs products increase with the quantity of 2-octyl-1-dodecanol in the aerosol (Figs. 2 and S6).

The observations, summarized in Fig. 2, are qualitatively consistent with the following set of reaction pathways: O_3 reacts with Tri to produce CI, which either decomposes to form OH and RO or reacts instead with the CI scavenger to form AAHs products. H-abstraction reactions by OH and RO lead to the formation of TriO and $TriO_2$. The relative importance of these two CI reaction pathways (unimolecular decomposition vs. bimolecular AAH

formation) is controlled by the quantity of the CI scavenger inside the aerosol.

Mass spectra (Fig. S7) are recorded for the Tri + O_3 reactions under wet (relative humidity = 60%) conditions since water reacts with CI to produce α-hydroxyalkyl hydroperoxide (HAH) products as shown in Fig. S4.[42,43] In the condensed phase, HAH is in equilibrium with a carbonyl and H_2O_2,[15,43,44] which are the products that are generally detected in many experiments rather than HAH. Consistent with previous observations,[15,22] increased relative humidity has no discernable effect on the global reactivity of Tri (i.e. γ_{eff}) as shown in Fig. 2A. This can be explained by OH regeneration from HAH as discussed in Refs.[43,44] and shown in Fig. 3B. Adding water to the reactor decreases the intensity of TriO and $TriO_2$ (Fig. 2B), which is similar to what is observed for the alcohol as discussed above. This is not surprising since H_2O and H_2O dimers, like 2-octyl-1-dodecanol, are efficient CI scavengers.

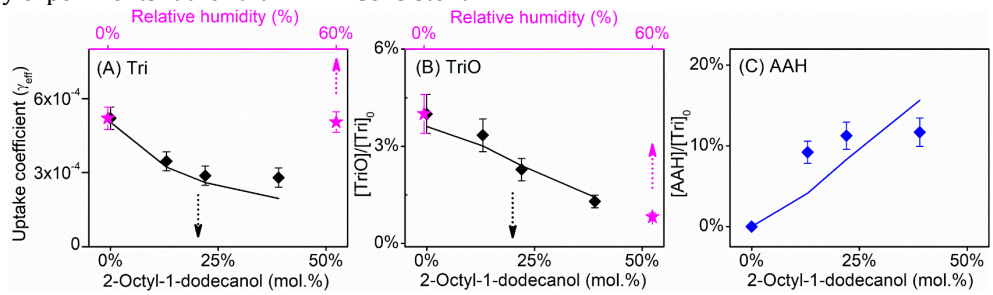

Figure 2. (A) Effective uptake coefficients (γ_{eff}) of cis-9-tricosene (Tri) and (B) the production of TriO, as a function of 2-octyl-1-dodecanol or relative humidity. (C) The production of α-alkoxyalkyl hydroperoxide (AHH) during ozonolysis ([O_3] ~ 4.0 × 10^{13} molecules·cm^{-3}) of aerosol comprised of varying amounts of Tri and 2-octyl-1-dodecanol. Symbols and solid lines are measured and simulated results, respectively.

The experimental observations presented above are explained qualitatively using the abbreviated reaction mechanism shown in Fig. 3. To simplify the discussion, the mechanism is divided into three parts (O_3, CI and OH / RO chemistries, Figs. 3A-C) each of which is characterized by a unique set of reaction products, pathways, and intermediate(s). The three sub-mechanisms (Figs. 3A-C) are linked by the formation and decomposition pathways of the CI. Electrophilic addition of ozone to the C=C bond of Tri forms a primary ozonide (POZ). The POZ decomposes into a CI and aldehyde co-product. Once formed, the CI can undergo bimolecular reactions with alcohol[38,39], H_2O[42,43] and O_3.[45] These bimolecular steps compete with unimolecular decomposition of the CI, which in the gas phase forms highly reactive OH and RO[36,37] that launch additional free radical reactions as shown in Fig. 3C.

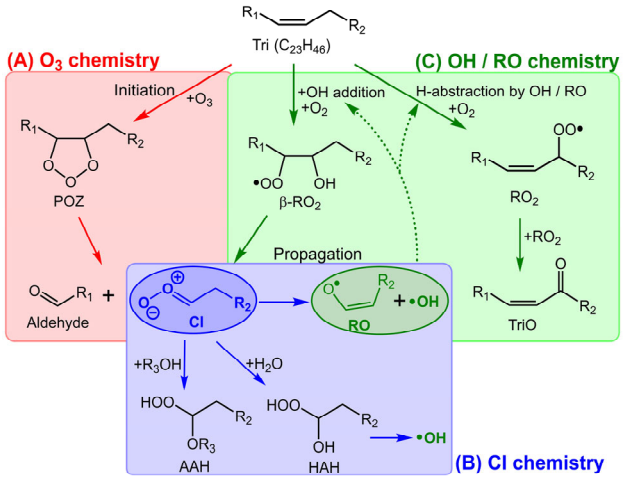

Figure 3. The three sub-mechanisms considered during the ozonolysis of cis-9-tricosene (Tri): (A) O_3, (B) Criegee intermediate (CI) and (C) hydroxyl (OH) / alkoxy (RO) radical reaction pathways. The reaction is initiated by Tri + O_3 to produce a primarily ozonide (POZ) then a CI. The propagation reactions mainly include the unimolecular bond scission of the CI to produce OH and RO, and the scission of β-hydroxy-peroxy radical (β-RO_2) to produce CI. The main termination reactions include bimolecular reactions of CI and bimolecular reactions of peroxy radicals (RO_2).

Once formed, OH reacts via two main pathways: H-abstraction from secondary or allylic C-H bonds in Tri/TriO and OH addition to the C=C of Tri/TriO (Fig. 3). RO reacts mainly by H-abstraction. These abstraction and addition reactions create two different peroxy radicals. H-abstraction, after O_2 addition, creates an RO_2 that leads to the formation of TriO and $TriO_2$, via RO_2 + RO_2 reactions, which terminate the radical chain. Alternatively, OH addition forms a β-hydroxy-peroxy (β-RO_2) radical as shown in Fig. 3 and discussed above. β-RO_2 is consumed via several possible reaction pathways. One pathway is a similar bimolecular self-reaction (i.e. β-RO_2 + RO_2) that terminates the radical chain by forming a stable hydroxy-ketone (or hydroxy-alcohol) product. Alternatively, unimolecular C-C bond scission of the β-RO_2 forms a CI (and an alkyl radical co-product) as first reported by Beauchamp and coworkers.[20,21] The CI can in turn react with alcohol or water, as discussed above, or decompose to regenerate OH and RO, which further propagates oxidation.

To quantitatively explain the experimental observations presented above, we construct a kinetic model based upon the mechanism outlined in Fig. 3. The model is intended to be predictive, so rate coefficients for the elementary reaction steps are constrained by prior literature or are computed using structure activity relationships (SAR), as shown in Table S1. Further information about the model, which includes a discussion of which reaction steps are included or excluded as well as details about the kinetic simulations can be found in the *Section S2 of Supporting Information*.

The only adjustable parameter in the model that is uncertain is the rate coefficient for β-RO_2 → CI, which is

assumed to be unimolecular (R13, Table S1). Although Beauchamp and coworkers[20,21] presented a plausible pathway for this reaction, which is mediated by O_2, further theoretical effort is needed to establish the exact mechanism (unimolecular vs. bimolecular), how it might be mediated by H_2O or neighboring molecules, barrier heights and rate coefficients.

The model predictions are compared to two independent data sets. First, the CI and OH/RO sub-mechanisms (shown in Figs. 3B and 3C) are compared to the Tri + OH measurements in the CFSTR reactor. This allows the portion of the model containing only OH reactions to be evaluated separately from the full model that includes elementary steps involving ozone. The model results and experimental data are compared in Figs. S11-S12. The model replicates the decay of Tri and the formation kinetics of TriO at three different [OH] (Fig. S11). In the model, Tri is consumed by three main pathways: gas/surface OH reactions, particle phase OH produced by decomposition of the CI and H-abstraction by RO. OH reacts both by H-abstraction as well as OH addition to C=C. The rate coefficients for these steps are from previous literature or are computed using SAR and the weighted distribution of reactive moieties in Tri. A sensitivity analysis for H-abstraction and OH addition is shown in Fig. S12. Changing the relative rates of H-abstraction vs. OH addition has a somewhat counter-intuitive effect on the predicted Tri decay kinetics, since H-abstraction ultimately leads to radical termination, whereas OH addition propagates the radical chain through the CI.

Ozone reaction steps are then added to the model and compared with the measured flow reactor kinetics for the Tri + O_3 reactions. As shown in Fig. S13, the agreement between the model and the observed decay of Tri is reasonable with some differences noted at high O_3 exposures. The model also replicates the formation kinetics of TriO during ozonolysis. Shown in Fig. 2 are model predictions of γ_{eff}, TriO and AAH as a function of 2-octyl-1-dodecanol (the CI scavenger) mole fraction. The model captures the overall trends in γ_{eff} and TriO observed in the experiments. Although the model captures the increase in AAH with increasing alcohol, there are some differences between simulation and experiment. One likely reason is missing AAH reaction steps, especially consumption pathways in the condensed phase, which require further study to provide better modeling constraints.

From the model we can estimate the main reactive sinks for Tri during ozonolysis, which yields insights into the importance of radical chain cycling in this model system. Shown in Fig. 4 are the consumption pathways for Tri as a function of 2-octyl-1-dodecanol mole fraction.

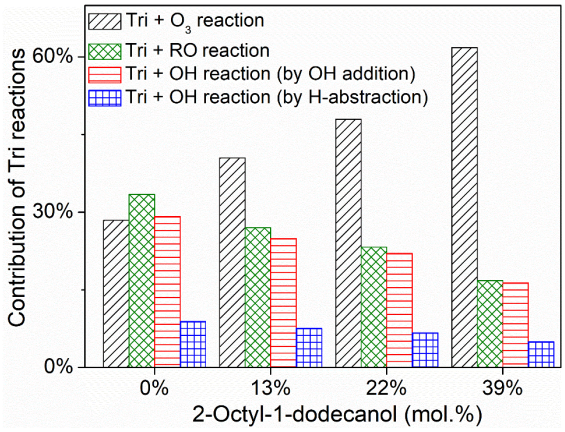

Figure 4. Relative contribution of reactions of cis-9-tricosene (Tri) with O_3, alkoxy radical (RO), and OH (addition and H-abstraction) as a function of 2-octyl-1-dodecanol mole fraction in the aerosol phase.

It can be seen in the Fig. 4 that increasing the alcohol fraction decreases the importance of OH and RO reactions during ozonolysis. At 39% alcohol, nearly ~ 60% of Tri is oxidized by O_3. This is because the bimolecular reaction of the CI with 2-octyl-1-dodecanol effectively outcompetes its unimolecular decomposition, which produces OH and RO (i.e. chain propagation). As the alcohol fraction is reduced, free radical reactions become more pronounced and Tri is increasingly consumed by OH and RO. Without alcohol to scavenge the CI, nearly 70% of the Tri reactions during ozonolysis are actually due to free radical oxidation. This is a surprising result that the dominant sink for Tri during ozonolysis is not O_3. This analysis reveals in a more detailed way how competitive pathways evolve and ultimately explains why there is a factor of ~ 2 decrease in measured γ_{eff} vs. alcohol fraction observed in Fig. 2.

Tri is an exceptional model system due to the location of its C=C bond. This is because an O_3 attack at this location produces relatively small volatile aldehydes that partition mainly to the gas phase. Evaporation of these aldehydes eliminates a significant condensed phase sink for CI, thereby enhancing the relative importance of unimolecular decomposition. In alkenes with differing structure, decomposition of the POZ would produce a CI and aldehyde co-product that both remain in the aerosol phase, which react to form a SOZ product.[15,22] Thus, the contribution of free radical oxidation to heterogeneous ozonolysis will depend sensitively on molecular structure, which is one important factor that controls the competition of unimolecular and bimolecular CI reaction pathways.

We find evidence for substantial radical chain cycling, which accounts for a substantial portion of the alkene reactivity and is driven by the coupling of CI and free radical oxidation pathways. These results further point to new mechanistic links between ozonolysis and free radical chain cycling. Once OH and RO are formed during ozonolysis, many of the free radical reaction pathways lead to radical termination and stable products (i.e. RO_2 + RO_2), while others cycle reactivity between CI and OH (i.e. O_3 + alkene → CI → OH → β-RO_2 → CI → OH → …), leading to more substantial heterogeneous oxidation of a surface or aerosol

than would be otherwise predicted when considering O_3 alone.

ASSOCIATED CONTENT

Supporting Information. This material is available free of charge via the Internet at http://pubs.acs.org.

Supporting information for experiments (Figs. S1 to S7) and simulations (Figs. S8 to S14, Tables S1 and S2).

AUTHOR INFORMATION

Corresponding Author

* Kevin R. Wilson (krwilson@lbl.gov)
ORCID: Kevin R. Wilson (0000-0003-0264-0872)

Notes

The authors declare no competing financial interest.

ACKNOWLEDGMENTS

The authors thank Bruce Rude for assistance at the ALS and Ryan S. Reynolds for helpful discussions. This work is supported by the Gas Phase Chemical Physics Program in the Chemical Sciences Geosciences and Biosciences Division of the Office of Basic Energy Sciences of the U.S. Department of Energy under Contract No. DE-AC02-05CH11231. This research used the Advanced Light Source, which is a U.S. Department of Energy Scientific User Facility under contract no. DE-AC02-05CH11231.

REFERENCES

(1) Jr., P. W.; Nieva, J.; Takeuchi, C.; Galve, R.; Wentworth, A. D.; Dilley, R. B.; DeLaria, G. A.; Saven, A.; Babior, B. M.; Janda, K. D.; Eschenmoser, A.; Lerner, R. A. Evidence for ozone formation in human atherosclerotic arteries. *Science* **2003**, 302, 1053-1056.

(2) Schneidemesser, E. v.; Monks, P. S.; Allan, J. D.; Bruhwiler, L.; Forster, P.; Fowler, D.; Lauer, A.; Morgan, W. T.; Paasonen, P.; Righi, M.; Sindelarova, K.; Sutton, M. A. Chemistry and the linkages between air quality and climate change. *Chem. Rev.* **2015**, 115, 3856-3897.

(3) Pöschl, U.; Shiraiwa, M. Multiphase chemistry at the atmosphere-biosphere interface influencing climate and public health in the anthropocene. *Chem. Rev.* **2015**, 115, 4440-4475.

(4) Gligorovski, S.; Abbatt, J. P. D. An indoor chemical cocktail. *Science* **2018**, 359, 632-633.

(5) Gligorovski, S.; Strekowski, R.; Barbati, S.; Vione, D. Environmental implications of hydroxyl radicals (•OH). *Chem. Rev.* **2015**, 115, 13051-13092.

(6) George, I. J.; Abbatt, J. P. Heterogeneous oxidation of atmospheric aerosol particles by gas-phase radicals. *Nat. Chem.* **2010**, 2, 713-722.

(7) Criegee, R. Mechanism of ozonolysis. *Angew. Chem. Int. Ed.* **1975**, 14, 745-752.

(8) Welz, O.; Savee, J. D.; Osborn, D. L.; Vasu, S. S.; Percival, C. J.; Shallcross, D. E.; Taatjes, C. A. Direct kinetic measurements of Criegee intermediate (CH_2OO) formed by reaction of CH_2I with O_2. *Science* **2012**, 335, 204-207.

(9) Taatjes, C. A.; Welz, O.; Eskola, A. J.; Savee, J. D.; Scheer, A. M.; Shallcross, D. E.; Rotavera, B.; Lee, E. P. F.; Dyke, J. M.; Mok, D. K. W.; Osborn, D. L.; Percival, C. J. Direct measurements of conformer-dependent reactivity of the Criegee intermediate CH_3CHOO. *Science* **2013**, 340, 177-180.

(10) Kroll, J. H.; Donahue, N. M.; Cee, V. J.; Demerjian, K. L.; Anderson, J. G. Gas-phase ozonolysis of alkenes: formation of OH from anti carbonyl oxides. *J. Am. Chem. Soc.* **2002**, 124, 8518-8519.

(11) Aschmann, S. M.; Arey, J.; Atkinson, R. OH radical formation from the gas-phase reactions of O_3 with a series of terpenes. *Atmos. Environ.* **2002**, 36, 4347–4355.

(12) Herrmann, F.; Winterhalter, R.; Moortgat, G. K.; Williams, J. Hydroxyl radical (OH) yields from the ozonolysis of both double bonds for five monoterpenes. *Atmos. Environ.* **2010**, 44, 3458-3464.

(13) Alam, M. S.; Camredon, M.; Rickard, A. R.; Carr, T.; Wyche, K. P.; Hornsby, K. E.; Monks, P. S.; Bloss, W. J. Total radical yields from tropospheric ethene ozonolysis. *Phys. Chem. Chem. Phys.* **2011**, 13, 11002-11015.

(14) Zhou, S.; Joudan, S.; Forbes, M. W.; Zhou, Z.; Abbatt, J. P. D. Reaction of condensed-phase Criegee intermediates with carboxylic acids and perfluoroalkyl carboxylic acids. *Environ. Sci. Technol. Lett.* **2019**, 6, 243-250.

(15) Heine, N.; Houle, F. A.; Wilson, K. R. Connecting the elementary reaction pathways of Criegee intermediates to the chemical erosion of squalene interfaces during ozonolysis. *Environ. Sci. Technol.* **2017**, 51, 13740-13748.

(16) Zhao, Z.; Xu, Q.; Yang, X.; Zhang, H. Heterogeneous ozonolysis of endocyclic unsaturated organic aerosol proxies: implications for Criegee intermediate dynamics and later-generation reactions. *ACS Earth Space Chem.* **2019**, 3, 344-356.

(17) Fooshee, D. R.; Aiona, P. K.; Laskin, A.; Laskin, J.; Nizkorodov, S. A.; Baldi, P. F. Atmospheric oxidation of squalene: molecular study using COBRA modeling and high-resolution mass spectrometry. *Environ. Sci. Technol.* **2015**, 49, 13304-13313.

(18) Chu, Y.; Cheng, T. F.; Gen, M.; Chan, C. K.; Lee, A. K. Y.; Chan, M. N. Effect of ozone concentration and relative humidity on the heterogeneous oxidation of linoleic acid particles by ozone: an insight into the interchangeability of ozone concentration and time. *ACS Earth Space Chem.* **2019**, 3, 779-788.

(19) Kenseth, C. M.; Huang, Y.; Zhao, R.; Dalleska, N. F.; Hethcox, J. C.; Stoltz, B. M.; Seinfeld, J. H. Synergistic O_3 + OH oxidation pathway to extremely low-volatility dimers revealed in beta-pinene secondary organic aerosol. *Proc. Natl. Acad. Sci. U.S.A.* **2018**, 115, 8301-8306.

(20) Zhang, X.; Barraza, K. M.; Beauchamp, J. L. Cholesterol provides nonsacrificial protection of membrane lipids from chemical damage at air-water interface. *Proc. Natl. Acad. Sci. U.S.A.* **2018**, 27, 3255-3260.

(21) Zhang, X.; Barraza, K. M.; Upton, K. T.; Beauchamp, J. L. Subtle changes in lipid environment have profound effects on membrane oxidation chemistry. *J. Am. Chem. Soc.* **2018**, 140, 17492-17498.

(22) Zeng, M.; Heine, N.; Wilson, K. R. Evidence that Criegee intermediates drive autoxidation in unsaturated lipids. *Proc. Natl. Acad. Sci. U.S.A.* **2020**, 117, 4486-4490.

(23) Zhou, Z.; Zhou, S.; Abbatt, J. P. D. Kinetics and condensed-phase products in multiphase ozonolysis of an unsaturated triglyceride. *Environ. Sci. Technol.* **2019**, 53, 12467-12475.

(24) Che, D. L.; Smith, J. D.; Leone, S. R.; Ahmed, M.; Wilson, K. R. Quantifying the reactive uptake of OH by organic aerosols in a continuous flow stirred tank reactor. *Phys. Chem. Chem. Phys.* **2009**, 11, 7885-7895.

(25) Wilson, K. R.; Jimenez-Cruz, M.; Nicolas, C.; Belau, L.; Leone, S. R.; Ahmed, M. Thermal vaporization of biological nanoparticles: fragment-free vacuum ultraviolet photoionization mass spectra of tryptophan, phenylalanine-glycine-glycine, and *b*-carotene. *J. Phys. Chem. A* **2006**, 110, 2106-2113.

(26) Smith, J. D.; Kroll, J. H.; Cappa, C. D.; Che, D. L.; Liu, C. L.; Ahmed, M.; Leone, S. R.; Worsnop, D. R.; Wilson, K. R. The heterogeneous reaction of hydroxyl radicals with sub-micron squalane particles: a model system for understanding the oxidative aging of ambient aerosols. *Atmos. Chem. Phys. Discuss.* **2009**, 9, 3945-3981.

(27) George, I. J.; Vlasenko, A.; Slowik, J. G.; Broekhuizen, K.; Abbatt, J. P. D. Heterogeneous oxidation of saturated organic aerosols by hydroxyl radicals: uptake kinetics, condensed-phase products, and particle size change. *Atmos. Chem. Phys.* **2007**, 7, 4187–4201.

(28) Wilson, K. R.; Smith, J. D.; Kessler, S. H.; Kroll, J. H. The statistical evolution of multiple generations of oxidation products in the photochemical aging of chemically reduced organic aerosol. *Phys. Chem. Chem. Phys.* **2012**, 14, 1468-1479.

(29) Bennett, J. E.; Summers, R. Product studies of the mutual termination reactions of sec-alkylperoxy radicals: evidence for non-cyclic termination. *Can. J. Chem.* **1974**, 52, 1377-1379.

(30) Russell, G. A. Deuterium-isotope effects in the autoxidation of aralkyl hydrocarbons. mechanism of the interaction of peroxy radicals[1]. *J. Am. Chem. Soc.* **1957**, 79, 3871-3877.
(31) Houle, F. A.; Hinsberg, W. D.; Wilson, K. R. Oxidation of a model alkane aerosol by OH radical: the emergent nature of reactive uptake. *Phys. Chem. Chem. Phys.* **2015**, 17, 4412-4423.
(32) Wiegel, A. A.; Wilson, K. R.; Hinsberg, W. D.; Houle, F. A. Stochastic methods for aerosol chemistry: a compact molecular description of functionalization and fragmentation in the heterogeneous oxidation of squalane aerosol by OH radicals. *Phys. Chem. Chem. Phys.* **2015**, 17, 4398-4411.
(33) Zhou, S.; Forbes, M. W.; Abbatt, J. P. Kinetics and products from heterogeneous oxidation of squalene with ozone. *Environ. Sci. Technol.* **2016**, 50, 11688-11697.
(34) Heine, N.; Arata, C.; Goldstein, A. H.; Houle, F. A.; Wilson, K. R. Multiphase mechanism for the production of sulfuric acid from SO_2 by Criegee intermediates formed during the heterogeneous reaction of ozone with squalene. *J. Phys. Chem. Lett.* **2018**, 9, 3504-3510.
(35) Pankow, J. F. An absorption model of gas/particle partitioning of organic compounds in the atmosphere. *Atmos. Environ.* **1994**, 28, 185-188.
(36) Li, H.; Kidwell, N. M.; Wang, X.; Bowman, J. M.; Lester, M. I. Velocity map imaging of OH radical products from IR activated $(CH_3)_2COO$ Criegee intermediates. *J. Chem. Phys.* **2016**, 145, 104307.
(37) Liu, F.; Beames, J. M.; Petit, A. S.; McCoy, A. B.; Lester, M. I. Infrared-driven unimolecular reaction of CH_3CHOO Criegee intermediates to OH radical products. *Science* **2014**, 345, 1596-1598.
(38) McGillen, M. R.; Curchod, B. F. E.; Chhantyal-Pun, R.; Beames, J. M.; Watson, N.; Khan, M. A. H.; McMahon, L.; Shallcross, D. E.; Orr-Ewing, A. J. Criegee intermediate–alcohol reactions, a potential source of functionalized hydroperoxides in the atmosphere. *ACS Earth Space Chem.* **2017**, 1, 664-672.
(39) Watson, N. I.; Black, J. A.; Stonelake, T. M.; Knowles, P. J.; Beames, J. M. An extended computational study of Criegee intermediate - alcohol reactions. *J. Phys. Chem. A* **2019**, 123, 218-229.
(40) Jacobs, M. I.; Xu, B.; Kostko, O.; Heine, N.; Ahmed, M.; Wilson, K. R. Probing the Heterogeneous Ozonolysis of Squalene Nanoparticles by Photoemission. *J. Phys. Chem. A* **2016**, 120, 8645-8656.
(41) Wells, J. R.; Morrison, G. C.; Coleman, B. K. Kinetics and Reaction Products of Ozone and Surface-Bound Squalene. *J. ASTM Int.* **2008**, 5, 1-12.
(42) Long, B.; Bao, J. L.; Truhlar, D. G. Unimolecular reaction of acetone oxide and its reaction with water in the atmosphere. *Proc. Natl. Acad. Sci. U.S.A.* **2018**, 115, 6135-6140.
(43) Hasson, A. S.; Chung, M. Y.; Kuwata, K. T.; Converse, A. D.; Krohn, D.; Paulson, S. E. Reaction of Criegee intermediates with water vapors - an additional source of OH radicals in alkene ozonolysis? *J. Phys. Chem. A* **2003**, 107, 6176-6182.
(44) Kumar, M.; Busch, D. H.; Subramaniam, B.; Thompson, W. H. Role of tunable acid catalysis in decomposition of a-hydroxyalkyl hydroperoxides and mechanistic implications for tropospheric chemistry. *J. Phys. Chem. A* **2014**, 118, 9701-9711.
(45) Vereecken, L.; Harder, H.; Novelli, A. The reactions of Criegee intermediates with alkenes, ozone, and carbonyl oxides. *Phys. Chem. Chem. Phys.* **2014**, 16, 4039-4049.

Table of Contents Graphic

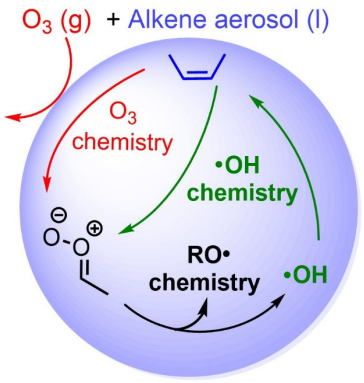

Supporting information for

Efficient Coupling of Reaction Pathways of Criegee Intermediates and Free Radicals in the Heterogeneous Ozonolysis of Alkenes

*Meirong Zeng and Kevin R. Wilson**

Chemical Sciences Division, Lawrence Berkeley National Laboratory, Berkeley, CA 94720, USA.

Corresponding Author*: Kevin R. Wilson (email: krwilson@lbl.gov)

Contents:

S1. Supporting information for experiments

S1.1. Experimental setup

The experimental setup consists of three main parts: (1) plumbing and instrumentation that feeds gas and particles to the (2) reactor and (3) particle and mass spectrometry detectors used to quantify heterogeneous kinetics. Detailed descriptions can be found in prior references so only a brief overview will be provided here.[1-3]

Polydisperse liquid aerosols are produced by passing dry N_2 through a heated Pyrex tube, located in a temperature-controlled furnace. The Pyrex tube is filled with liquid cis-9-tricosene (Tri, Sigma-Aldrich, 97% pure) or mixed with 2-octyl-1-dodecanol (Sigma-Aldrich, 97% pure). The furnace temperatures are adjusted for each experiment to generate stable droplets (~ 110 °C for pure Tri aerosols and several degrees lower for the Tri/2-octyl-1-dodecanol mixtures). Residual gas-phase organics are removed prior to the reactor by passing the aerosols/N_2 flow through an annular activated charcoal denuder. The aerosol flow is then mixed with gas flows that include the oxidants (i.e. H_2O_2 or O_3), O_2 and humidified (or dry) N_2.

For ozonolysis, the mixture of aerosols and gases (O_3, O_2, humidified or dry N_2) are introduced into a flow reactor (Fig. S1) with an average residence time of ~ 37 seconds at a total flow of 1.1 SLM. O_3 is produced by passing 0.05-SLM O_2 through a corona discharge generator, which is diluted by dry N_2 (3 SLM). The O_3 concentration (0 – 10 ppm) is then measured with an ozone monitor (2B technology model 202M).

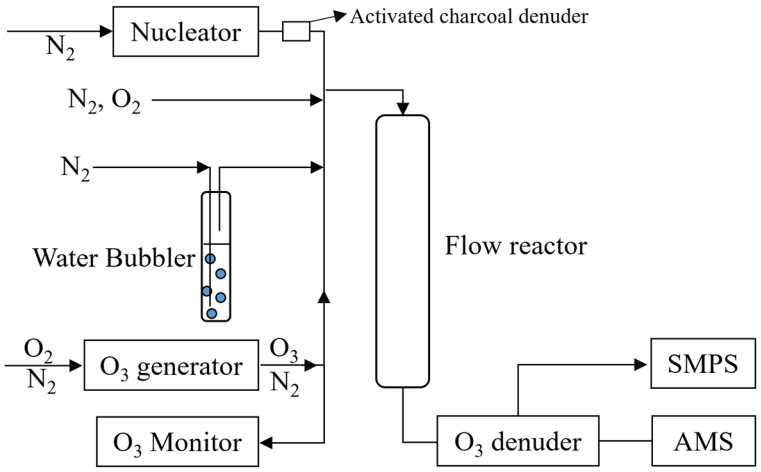

Figure S1. A schematic view of the flow reactor used in the heterogeneous ozonolysis experiments. The SMPS and AMS are scanning mobility particle sizer and aerosol mass spectrometer, respectively.

For the OH oxidation experiments, the mixture of aerosols and gases (H_2O_2, O_2, humidified or dry N_2, OH tracer) are introduced into a continuous flow stirred tank reactor (CFSTR) as shown in Fig. S2. OH is generated *in situ* by the photolysis of gas-phase H_2O_2 (< 10 ppm) using UV lamps ($\lambda \sim 356$ nm). H_2O_2 vapor is generated by passing the dry N_2 (0.1 SLM) through a heated bubbler (60 °C) containing a 50/50 mixture urea-hydroperoxide ($CO[NH_2]_2 \cdot H_2O_2$, Sigma-Aldrich, 97% pure) and sand (SiO_2, 50–70 mesh particle size, Sigma-Aldrich). The concentration of gas-phase H_2O_2 in the CFSTR after ~ 2 hours of filling is several ppm (<10 ppm), which is measured by a Vaisala H_2O_2 sensor (HPP272). Gas-phase 2-methyl-2-butene (< 200 ppb) is introduced as a tracer to quantify the average OH concentration in the reactor.[1,4] The total flow rate through the CFSTR was kept at ~1.1 SLM, yielding reaction times of hours.

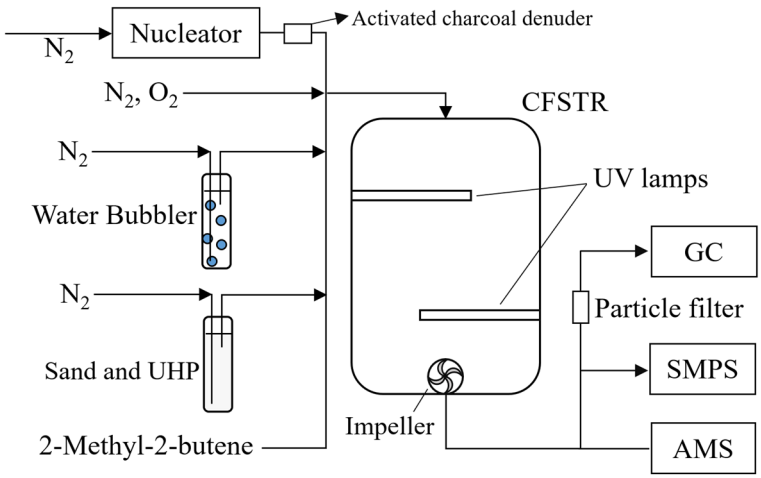

Figure S2. A schematic view of the continuous flow stirred tank reactor (CFSTR) used in the heterogeneous OH oxidation experiments. The UHP in the bubbler is urea-hydroperoxide. The GC, SMPS and AMS are gas chromatograph, scanning mobility particle sizer, and aerosol mass spectrometer, respectively.

The reactions are monitored using three detectors. The particle-size distribution is measured by a scanning mobility particle sizer (SMPS, TSI 3080L DMA and 3025A CPC). The decay of the gas-phase tracer, 2-methyl-2-butene, is measured using a gas chromatograph (GC, SRI Instruments 8610C with FID detection). The chemical composition of the aerosol is measured using a home-made vacuum ultraviolet aerosol mass spectrometer (VUV-AMS)[5] located at the Chemical Dynamics Beamline (9.0.2), Advanced Light Source (ALS), Lawrence Berkeley National Laboratory, Berkeley, CA, USA. Due to the lack of photoionization cross-sections and ion fragmentation patterns, it is very hard to measure absolute concentrations of products. Instead, we use relative abundance (%). The relative abundance for species X is normalized by the unreacted Tri (i.e. $[X]/[Tri]_0$) signal, which is used to compare with the simulated results produced by our kinetic model. Reaction products with mass-to-charge-ratio (m/z) < 200 are not shown since it is difficult to distinguish smaller reaction products from ion fragments of larger species produced by dissociative photoionization (e.g. possible ion fragments from α-alkoxyalkyl hydroperoxides

shown in Figs. S3 and S5). Additionally, smaller reaction products in this mass range are expected to be too volatile to remain in the aerosol. This experimental setup has been used extensively in prior studies of heterogeneous reactions and further details can be found in Refs.[2-4,6].

S1.2. Reaction scheme and product identification

As shown in Figs. 3 and S3, ozonolysis of Tri ($C_{23}H_{46}$) begins by the electrophilic addition of O_3 to the C=C bond in Tri. This produces a primary ozonide (POZ, $C_{23}H_{46}O_3$), that undergoes bond scission to produce a C_{14} aldehyde ($C_{14}H_{28}O$) and a C_9 CI ($C_9H_{18}O_2$), or a C_9 aldehyde ($C_9H_{18}O$) and a C_{14} CI ($C_{14}H_{28}O_2$). The C_9 and C_{14} aldehydes are volatile and evaporate easily into gas phase. The C_9 and C_{14} CI can react with H_2O to produce α-hydroxyalkyl hydroperoxides (HAH), which can be consumed via three unimolecular pathways[7,8] as shown for the C_{14} CI in Fig. S4. Bimolecular reactions of the C_9 CI and the C_{14} CI with the CI scavenger (2-octyl-1-dodecanol, $C_{20}H_{42}O$) produce two α-alkoxyalkyl hydroperoxides: $C_{29}H_{60}O_3$ (C_{29} AAH) and $C_{34}H_{70}O_3$ (C_{34} AAH), respectively.

AAH products are not detected as parent ions but at *m/z's* corresponding the elimination of H_2O and H_2O_2 as described in Ref.[2] and shown in Fig. S3. The C_{34} AAH product exhibits additional fragmentation pathways as shown in Fig. S5. 2-Octyl-1-dodecanol is also not detected as its parent molecular ion ($C_{20}H_{42}O$, *m/z* = 298) but instead at a *m/z* corresponding to -H_2O loss ($C_{20}H_{40}$, *m/z* = 280). Unfortunately, as shown in Fig. S5, the C_{34} AAH also has a fragment at *m/z* = 280, which prevents us from measuring the kinetic evolution of 2-octyl-1-dodecanol during the Tri + O_3 experiments. As previously noted, fragmentation in VUV aerosol mass spectra is quite sensitive to the aerosol vaporization temperature and photoionization energy.[5]

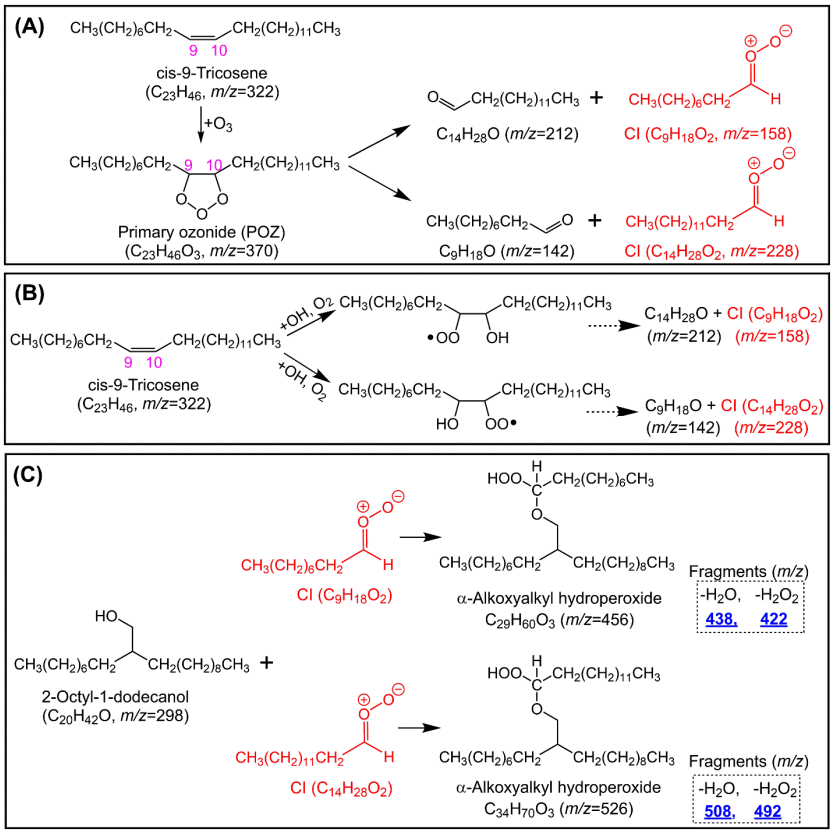

Figure S3. (**A**) Reaction pathways of cis-9-tricosene and ozone to produce CI and aldehydes. (**B**) Reaction pathways of cis-9-tricosene and OH to produce CI and aldehydes. (**C**) Reactions pathways of the CI scavenger (2-octyl-1-dodecanol) to produce two α-alkoxyalkyl hydroperoxides. Also shown are the *m/z's* used for assignment in VUV-AMS mass spectrum.

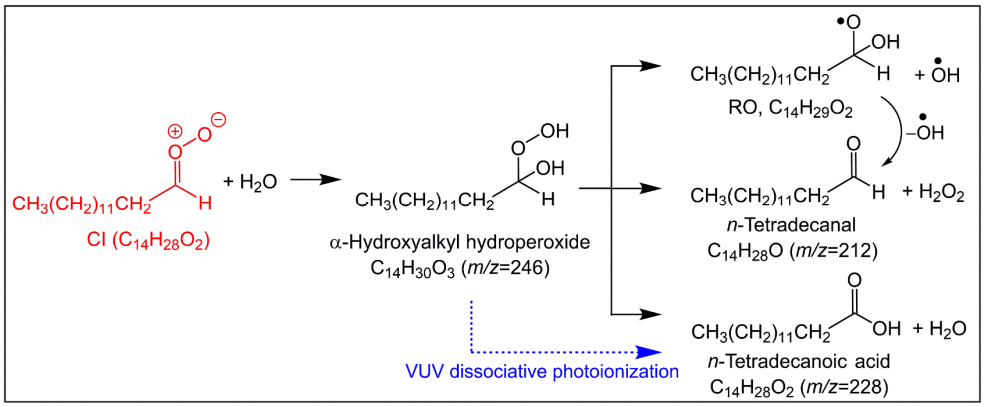

Figure S4. The reaction pathway of C_{14} CI with H_2O produces the C_{14} α-hydroxyalkyl hydroperoxide (C_{14} HAH) and three unimolecular decomposition pathways of the C_{14} HAH. VUV dissociative photoionization of C_{14} HAH can also generate the n-tetradecanoic acid and H_2O as indicated by blue arrow.

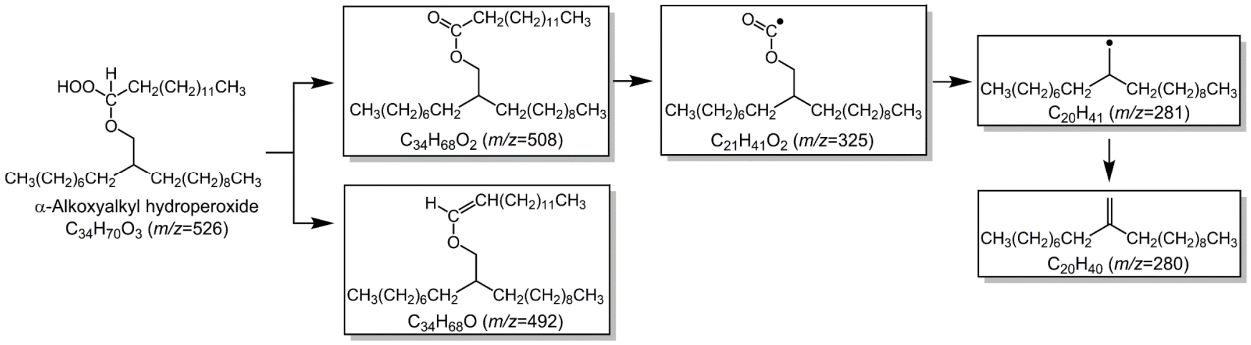

Figure S5. Fragmentation pathways of the C_{34} α-alkoxyalkyl hydroperoxide. Fragment *m/z*'s are shown to justify their assignment in the VUV-AMS mass spectrum. Fragments are likely produced by dissociative photoionization.

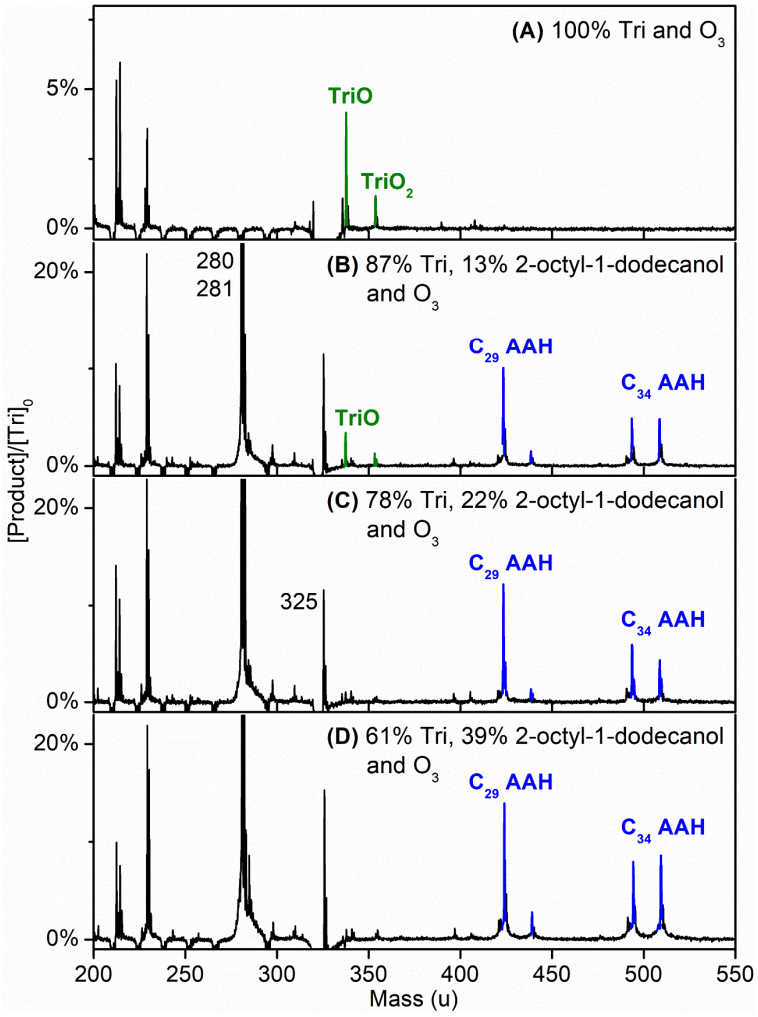

Figure S6. Difference mass spectra (unreacted Tri – reacted Tri) showing the major reaction products, such as ketone (TriO and $TriO_2$) and α-alkoxyalkyl hydroperoxide (AHH) during (**A**) the 100% Tri + O_3 reactions; (**B**) 87% Tri, 13% 2-octyl-1-dodecanol + O_3 reactions; (**C**) 78% Tri, 22% 2-octyl-1-dodecanol + O_3 reactions; (**D**) 61% Tri, 39% 2-octyl-1-dodecanol + O_3 reactions.

S1.3. Relative humidity dependence for Tri + O_3 reactions

As shown in Fig. S7, the Tri + O_3 reaction is measured under dry and wet (relative humidity = 60%) conditions. As discussed in the main text, the concentrations of TriO and $TriO_2$ decrease with the addition of water vapor (Figs. 2B, S7A-S7B) since H_2O acts as a CI scavenger via the bimolecular reaction shown in Fig. 3. However, in the presence of particle-phase alcohol, relative humidity does not change the observed intensities of the α-alkoxyalkyl hydroperoxide (AAH) products (Figs. S7C-S7D). This shows that 2-octyl-1-dodecanol is a more effective CI scavenger than water.

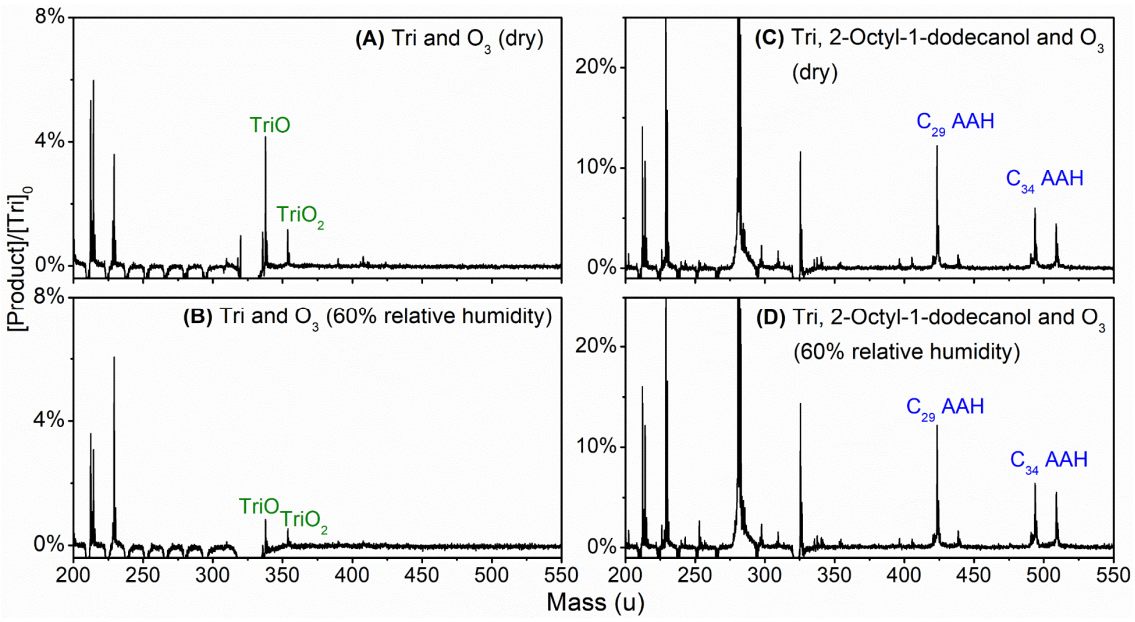

Figure S7. Difference VUV-AMS spectra (unreacted Tri – reacted Tri) observed in the Tri + O_3 reactions (A and B), and spectra recorded for the Tri/2-octyl-1-dodecanol + O_3 reactions (C and D) under dry conditions and at 60% relative humidity ($[O_3] \sim 4.0 \times 10^{13}$ molecules·cm^{-3}).

S2. Supporting information for simulations

S2.1. Simulation methods and model development

A chemical kinetic model is developed in Kinetiscope©[9], which had been used extensively to model heterogeneous chemical reactions.[3,10-16] As shown previously for heterogeneous reactions with OH[11-13,15,16] and O_3[3,14], a single instantaneously mixed compartment is used to represent the aerosol, which is a valid assumption for a liquid that is well-mixed on reaction timescales.[10] To properly account for surface-to-volume scaling in the spherical aerosols, the single compartment is represented by a 1 nm × 1 nm × (R/3) nm rectangular volume, where R is the measured radius of the aerosol. Gas-phase O_3 (or OH) adsorption occurs in a 1 nm thick surface region as discussed in Ref.[3]. The model is comprised of three parts: (a) the adsorption of gas-phase O_3 (or OH) onto the surface of the aerosol; (b) condensed-phase chemical reactions and (c) evaporation of volatile products, such as the volatile aldehydes ($C_{14}H_{28}O$ and $C_9H_{18}O$) in Fig. S3. How evaporation has been previously modeled is described in prior studies.[3,13]

(a) Adsorption of gas-phase O_3 (or OH)

Here we assume a Langmuir Hinshelwood mechanism, where OH or O_3 adsorbs to the surface prior to reaction and that there is one adsorption site per molecule. A pseudo-first order rate coefficient (k_{ads}) is used to describe the adsorption of O_3 (or OH) onto the surface of the aerosols by using equations S1 for O_3, and S2 for OH, respectively.

$$k_{ads,O_3} = [O_3] \times Z \times S_{O_3} \quad \text{(S1)}$$

$$k_{ads,OH} = [OH] \times Z \times S_{OH} \quad \text{(S2)}$$

Here, [O_3] and [OH] are the measured concentrations used in the experiment. Z is the collision frequency of O_3 (or OH), which is $\sigma \times \nu$. σ is the collision cross-section of the surface (1 nm × 1 nm) and ν is the mean speed of ozone (390 $m \cdot s^{-1}$) or OH (610 $m \cdot s^{-1}$). S is the sticking coefficient of O_3 (or OH). The sticking coefficient of O_3 (S_{O_3}) used in the model is 2.4×10^{-5}, which is within the range ($10^{-5} \sim 10^{-4}$) reported in the Refs.[17,18]. It is smaller than the value (1.8×10^{-4}) used previously to model the Sqe + O_3 reaction[3] and is roughly consistent with the difference in the number of C=C bonds in Sqe (6 C=C bonds) vs. Tri. The sticking coefficient of OH (S_{OH}) used in present model is estimated to be 0.2, in order to achieve a global agreement between simulations and experiments as shown in Fig. S11. The rate constants for the adsorption are shown in Table S1.

(b) Condensed-phase chemical reactions

Shown in Table S1 are the elementary reaction steps used in the model, which reflect the three sub-mechanisms shown schematically in Fig. 3. A discussion and analysis of additional reactions that are not included in the model can be found in Section S2.2. References for the rate coefficients are also shown in Table S1. We use the general notation of RH to represent stable molecules (e.g. RH = Tri). The sub-mechanism for the heterogeneous ozonolysis of alkenes is quite well-known and is taken from prior work.[3,14,19,20] One lumped reaction step (R1), which neglects the explicit formation/decomposition of the POZ, is used to form the CI and aldehyde (C=O) consistent with previous models of ozonolysis.[3]

The CI is consumed via four main pathways (R2-R5). The unimolecular reaction of CI produces an alkoxy radical (RO) and OH (R2). Bimolecular steps of CI include reaction with the CI scavenger (2-octyl-1-dodecanol, ROH) to produce α-alkoxyalkyl hydroperoxide (AAH),

reaction with O_3 produce a ketone (C=O), and reaction with H_2O produce α-hydroxyalkyl hydroperoxide (HAH). The consumption pathways of HAH are mainly its unimolecular reaction to produce an RO and OH, or to produce ketone and H_2O_2.[7,8] The bimolecular reaction of CI with aldehydes to produce a secondary ozonide (SOZ) is neglected since they are not detected in the experiment.

The radical sub-mechanism includes OH, alkoxy (RO) and peroxy (RO_2) radical reactions (R6-R13). Elementary OH steps include H-abstraction (R6) and OH-addition (R7). H-abstraction by RO is shown in step R8. The addition of RO to Tri is not considered since the experiment yielded no evidence for products that would be produced by this reaction.

The alkyl radical (R), produced by H-abstraction reactions, and the hydroxy alkyl radical (R_OH), produced from the OH-addition reactions, contribute to the formation of peroxy radical (RO_2) and β-hydroxy-peroxy radical (β-RO_2), respectively. O_2 addition to these alkyl radicals, is described as pseudo first order, as shown in R9 and R10. Peroxy radical steps include self-reactions (i.e. $RO_2 + RO_2$) form stable ketone and alcohol (R11) products or two alkoxy radicals (R12).

The β-hydroxy-peroxy radical (β-RO_2) decomposes to form a CI (R13) as reported by Beauchamp and coworkers.[21,22] However, we lack theoretical calculations or experiments to constrain this rate constant. Thus this is an adjustable parameter in the model. We assume this step is unimolecular and a value of 120 s^{-1} produces model results in reasonable agreement with the global data set. We note that H_2O (or O_2) could facilitate this reaction as suggested in Ref.[21]. Thus, further theoretical study is needed to provide more stringent constrains for this reaction step.

Table S1. Reaction scheme and rate coefficients for stochastic simulations.

No.	Reactions	Rate constant	Notes
	O_3 gas → O_3_ads	0.37 s^{-1}	*a*
	OH gas → OH_ads	1.96×10^{-3} s^{-1}	*a*
R1	RH + O_3 → CI + C=O	2.00×10^{-16} $cm^3 \cdot molec.^{-1} \cdot s^{-1}$	*Ref.[3]*
R2	CI → RO + OH	205 s^{-1}	*Ref.[23]*
R3	CI + ROH → AAH	6.70×10^{-19} $cm^3 \cdot molec.^{-1} \cdot s^{-1}$	*b*
R4	CI + O_3 → C=O	4.00×10^{-13} $cm^3 \cdot molec.^{-1} \cdot s^{-1}$	*Ref.[3]*
R5	CI + H_2O → HAH	2.17 s^{-1}	*c*
Triggered radical chemistry			
R6	RH + OH → R + H_2O	2.00×10^{-11} $cm^3 \cdot molec.^{-1} \cdot s^{-1}$	*d*
R7	RH + OH → R_OH	6.60×10^{-11} $cm^3 \cdot molec.^{-1} \cdot s^{-1}$	*Ref.[24]*
R8	RH + RO → R + ROH	1.66×10^{-15} $cm^3 \cdot molec.^{-1} \cdot s^{-1}$	*Ref.[25]*
R9	R + O_2 → RO_2	1.10×10^{6} s^{-1}	*e*
R10	R_OH + O_2 → β-RO_2	1.10×10^{6} s^{-1}	*e*
R11a	RO_2 + RO_2 → RC=O + ROH	4.00×10^{-15} $cm^3 \cdot molec.^{-1} \cdot s^{-1}$	*Ref.[25]*
R11b	β-RO_2 + β-RO_2 → RC=O + ROH	4.00×10^{-15} $cm^3 \cdot molec.^{-1} \cdot s^{-1}$	*Ref.[25]*
R12	RO_2 + RO_2 → RO + RO + O_2	1.00×10^{-16} $cm^3 \cdot molec.^{-1} \cdot s^{-1}$	*Ref.[25]*
R13	β-RO_2 → CI + R_OH	120 s^{-1}	*f*

Note: [a]Rate coefficients depend on the [OH] or [O_3] concentration; [b]Rate coefficient is the same as the reaction of CI with aldehydes to produce secondary ozonides from Ref.[3]; [c]Treated as pseudo-first-order rate constant where [H_2O] = 3% for dry condition, $k = 4.3 \times 10^{-15}$ $cm^3 \cdot molec.^{-1} \cdot s^{-1}$ from Ref.[23]. [d]Rate coefficients for the H-abstraction reaction are calculated from the structure-activity relationship (SAR) in Refs.[26,27], such as 2.00×10^{-11} $cm^3 \cdot molec.^{-1} \cdot s^{-1}$ for Tri and OH. [e]Treated as pseudo-first-order rate constant where [O_2] = 10%, $k = 2.5 \times 10^{-12}$ $cm^3 \cdot molec.^{-1} \cdot s^{-1}$ from Refs.[10,25]. [f]*Estimated in this work, see text for details.*

S2.2. Additional mechanistic tests of the model

In addition to the reactions included in the base model shown in Table S1 (Section S2.1), below we evaluate the possible importance of a number of other pathways involving CI, RO_2 and

RO. These steps are shown in Table S2 and are denoted Test_R1-5. These reaction steps are individually added to the base model (Table S1) to produce a new test model. The relative kinetic importance of these reactions are then evaluated by comparing the output from the test model with experimental observations and the base model predictions as discussed below.

Table S2. Additional reaction types (named as Test_R) and rate coefficients used in the test model.

No.	Reactions in Test model	Rate constant	Notes
Test_R1	CI + Tri → CHP	7.0×10^{-16} $cm^3 \cdot molec.^{-1} \cdot s^{-1}$	*Ref.*[28]
Test_R2	RO_2 + Tri → RO + Epoxide	1.66×10^{-21} $cm^3 \cdot molec.^{-1} \cdot s^{-1}$	*Ref.*[29]
Test_R3	RO_2 + Tri → ROOH + Tri_R	2.3×10^{-21} $cm^3 \cdot molec.^{-1} \cdot s^{-1}$	*Ref.*[25]
Test_R4	Tri_RO_2 → Tri_QOOH	5×10^{-4} s^{-1}	*Ref.*[30]
Test_R5	RO → Unimolecular decomposition	*See text*	*Refs.*[31,32]

Reaction of CI with alkenes. In the gas phase CI react with alkenes to produce a five membered cyclic hydroperoxide (CHP).[28,33] Given the high concentration of Tri in the particle we evaluate the potential importance of these reactions for the present work shown as Test_R1 in Table S2. The reaction of the C_9 and C_{14} CI ($C_9H_{18}O_2$ and $C_{14}H_{28}O_2$, Fig. S3) with Tri ($C_{23}H_{46}$) would produce a C_{32} CHP and C_{37} CHP, i.e. $C_9H_{18}O_2 + C_{23}H_{46} \rightarrow C_{32}H_{64}O_2$; and $C_{14}H_{28}O_2 + C_{23}H_{46} \rightarrow C_{37}H_{74}O_2$. These two reactions are added to the base model (Table S1) and a new simulation is conducted (termed test model). The rate constant used for these steps is 7.0×10^{-16} $cm^3 \cdot molec.^{-1} \cdot s^{-1}$ as reported in Ref.[28] As shown in Fig. S8, the simulated concentrations of TriO and AAH in the test model are much lower (i.e. near zero) than experimental observations and the predictions of the base model, which lacks the CI + Tri reaction. As shown with reaction step markers in Fig. S8A, the consumption of the CI is dominated by the CI + Tri reactions. When included the CI + Tri pathways outcompete unimolecular decomposition of the CI, effectively

shutting off free radical production, which is the source of TriO as shown in Figs. S8A and S8B. This is also the case for AAH production shown in Fig. S8C, where the reactions of CI + 2-octyl-1-dodecanol cannot compete with Tri + CI.

We find no evidence for the production of the C_{32} CHP (*m/z* = 480) and C_{37} CHP (*m/z* = 550) products in the mass spectrum (e.g. Fig. 1). This is consistent with many previous studies, which do not report evidence for this reaction or the formation of CHP during the heterogeneous ozonolysis of unsaturated compounds.[3,19,20,34-36] Thus, these reaction steps are not included in the base model shown in Table S1.

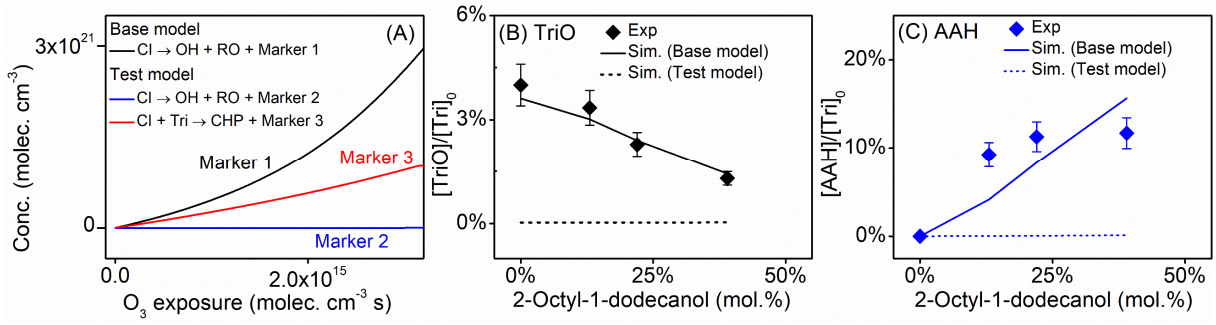

Figure S8. (**A**) Simulated concentrations and reaction markers for two competitive consumption pathways of CI in the base model (Table S1), and the test model (Table S1 + (Tri + CI reactions)) during the Tri + O_3 reactions. (**B** and **C**) Experimental (symbols) and simulated (lines) concentrations of TriO and AAH. Solid and dash lines are simulations by the base model and test model, respectively.

Reaction of RO_2 with alkenes. RO_2 can react with an alkene to produce a RO and epoxide as discussed in Ref.[29]. To evaluate the effects of including this reaction type in the simulations, the reactions of RO_2 with Tri to produce a RO and an epoxide (i.e. RO_2 + Tri → RO + epoxide, Test_R2 in Table S2) are added to the base model. The rate constant for this reaction type is 1.66×10^{-21} $cm^3 \cdot molec.^{-1} \cdot s^{-1}$ from Ref.[29]. The results of simulations with and without this reaction type are nearly identical as shown in Fig. S9A. For example, the relative contribution of the RO_2 + Tri reactions to the consumption of Tri is ~ 0.5%, compared with contributions from other reactions

(Fig. 4), i.e. the Tri + O_3, Tri + OH, and Tri + RO reactions. The relative contribution of this reaction type to the consumption of RO_2 is ~ 1%, compared with competing reactions such as the bimolecular reaction of two RO_2. The concentration of the epoxide from this reaction type is also negligible. Given that this reaction type plays a minor role under our experimental conditions, we have not included this reaction type in the base model shown in Table S1.

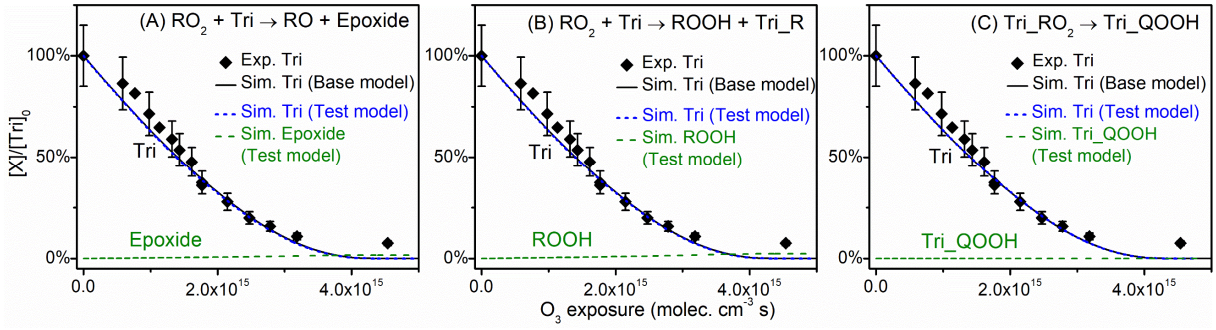

Figure S9. Experimental (symbols) and simulated (lines) concentrations of Tri, (**A**) Epoxide, (**B**) ROOH and (**C**) Tri_QOOH during the Tri + O_3 reactions. Solid lines are simulations by the base model. Dash lines are simulations by the test model, which includes (**A**) Test_R2, RO_2 + Tri → RO + Epoxide; (**B**) Test_R3, RO_2 + Tri → ROOH + Tri_R; (**C**) Test_R4, Tri_RO_2 → Tri_QOOH, respectively.

H-abstraction by RO_2. H-abstraction reactions of organic molecules by RO_2 (e.g. Tri) produce a hydroperoxide (ROOH) and alkyl radical (R) as discussed in Refs.[25,37,38] To test the importance of this reaction type in the simulations under our reaction conditions, the reactions of the RO_2 with Tri to produce the ROOH and the Tri alkyl radical (i.e. RO_2 + Tri → ROOH + Tri_R, Test_R3 in Table S2) are added to the base model shown in Table S1. The rate constant (2.3×10^{-21} $cm^3 \cdot molec.^{-1} \cdot s^{-1}$) is estimated from Ref.[25] The inclusion of these reaction steps do not alter the predictions of the base model as shown in Fig. S9B. For example, the relative contributions of this reaction type (RO_2 + Tri) to the consumption of RO_2 and Tri are small (~ 1%). Thus, for simplicity these reactions are not included in the base model (Table S1).

Isomerization of RO_2 → QOOH. The isomerization reaction of RO_2, via an internal H-shift, can produce a hydroperoxyalkyl radical (QOOH) as discussed in Refs.[30,39]. To test the effects of including this reaction type (Test_R4 in Table S2), the isomerization of Tri peroxy radical (Tri_RO_2) to produce a Tri hydroperoxyalkyl radical (Tri_QOOH) is added into a test model using the rate constant (5×10^{-4} s^{-1}) from Ref.[30] Test model simulations show that the relative contribution of this reaction to the consumption of Tri_RO_2 is negligible (~ 0%), compared with the competing bimolecular Tri_RO_2 + RO_2 (e.g. Tri_RO_2) reactions. The simulated concentration of Tri_QOOH by the test model is also negligible (~ 0%) as shown in Fig. S9C.

Unimolecular decomposition of RO. The unimolecular decomposition of the C_9 and C_{14} CI can produce OH and conjugated RO radicals as shown in Fig. S10. Three unimolecular decomposition reactions of RO are possible (Fig. S10 and Test_R5 in Table S2) based on Refs.[31,32] The β-C-C scission reaction of the C_9 RO to produce a hexyl (C_6 R) radical and acrolein (C_3H_4O) is similar to the β-C-C scission of n-butyl ($k = 1.2 \times 10^{-8}$ s^{-1} from Ref.[32]). The remaining two reactions, in Fig. S10, of the C_9 RO to produce $C_9H_{16}O$ and H, or to produce C_8H_{16} and HCO are analogous to C_3H_5O (CH_3CHCHO) reactions, which have rate coefficient of 1.66×10^{-22} and 3.5×10^{-18} s^{-1} from Ref.[31], respectively. As shown in R8 in Table S1, the rate constant for the bimolecular reaction of the RO with Tri via H-abstraction is 1.66×10^{-15} $cm^3 \cdot molecules^{-1} \cdot s^{-1}$. The pseudo-first-order rate constant for R8 is ~ 2.5×10^6 s^{-1} with the $[Tri]_0$ of 1.5×10^{21} $molec. \cdot cm^{-3}$. This rate is several orders of magnitude faster than the unimolecular decomposition reactions of RO (Fig. S10); showing that the main sink for RO, under our experimental conditions, is bimolecular H abstraction. Thus unimolecular decomposition reactions of RO were not included in the base model shown in Table S1.

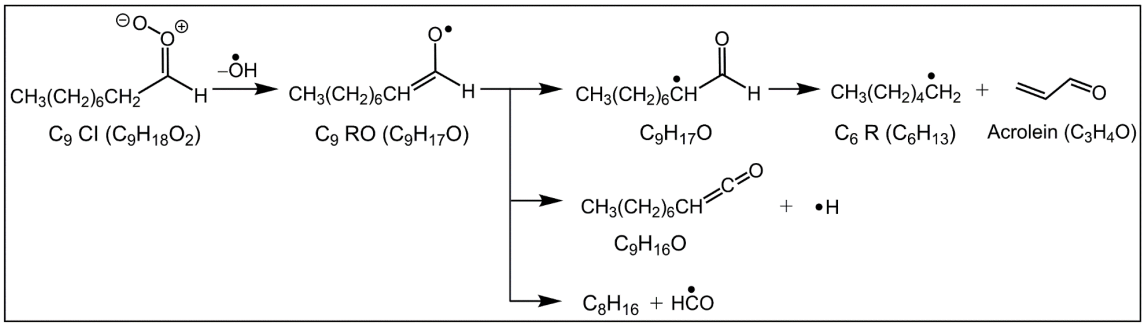

Figure S10. The unimolecular decomposition reaction of C_9 CI produces OH and the conjugated C_9 RO. Three unimolecular decomposition pathways of C_9 RO.

S2.3. Simulation results for Tri + OH reactions in the CFSTR

As discussed in the main text, in order to isolate radical reactions (OH-RO-RO_2) from O_3 chemistry, we first evaluate the model against the experimental observations for the Tri + OH reaction (without O_3). These experiments are conducted in a continuous flow stirred tank reactor (CFSTR). As described by Che et al.[1] and reviewed briefly here, measurements in the CFSTR occur in two steps. The reactor is first filled with the fresh reagents (aerosols, gas-phase H_2O_2, gas-phase tracer 2-methyl-2-butene, dry or humidified N_2, O_2) with lamps off. After a ~ 2 hours of filling, the lamps are turned on to initiate the reaction by the photolysis of H_2O_2 to produce OH. During the reaction there is a constant flow of reagents into the reactor as well as products and reactants exiting the reactor. Thus, in order account for this, two additional steps (S4 and S5) are added into the model to account for the continuous flow as described by Richards-Henderson et al.[15]. The rate constants for the flow process (S4 and S5) are the same (~ 10^{-4} s^{-1}) and are measured by quantifying the rate of increase of aerosol mass while filling an empty chamber[1].

$$\text{Fill} \rightarrow \text{Tri} + \text{Fill} \qquad \text{(S4)}$$

$$\text{Tri} \rightarrow \text{out} \qquad \text{(S5)}$$

The model prediction is compared to Tri + OH experiments conducted at three different [OH] in CFTSR as shown in Fig. S11. In the experiment, the peak in the mass spectrum corresponding to TriO appears to have two contributions: TriO ($C_{23}H_{44}O$) and a fragment ion produced by dissociative photoionization (-H_2O loss) of Tri_OH_CO ($C_{23}H_{46}O_2$). Thus to more closely compare with experiment, the modeled TriO species are a sum of tricosenyl ketone (TriO) and hydroxy-tricosenyl ketone (Tri_OH_CO) products. Overall, the model predictions are in reasonable agreement with experimental results.

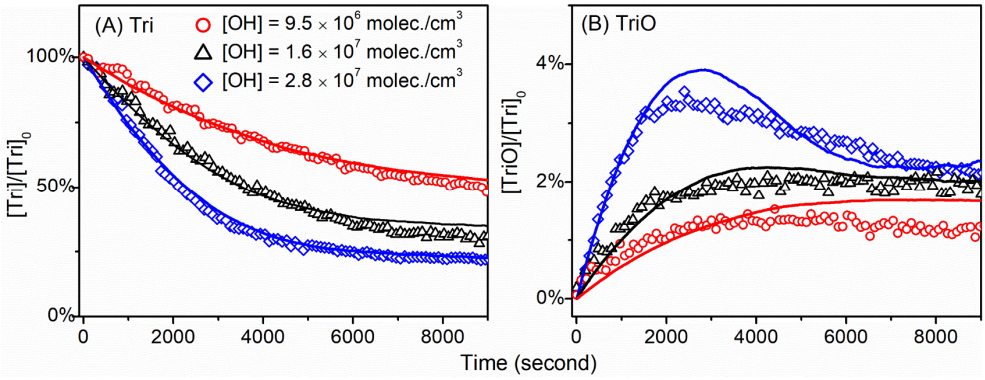

Figure S11. Experimental (symbols) and simulated (lines) concentrations of (A) Tri and (B) TriO in the CFSTR under various [OH].

A model sensitivity test is performed and shown in Fig. S12. The base model, shown in Table S1, uses SAR to compute OH addition and H-abstraction rate coefficients. These computed rate coefficients are changed by a factor of 5 and compared to the experimentally observed Tri decay at [OH] = 1.6×10^7 molecules cm^{-3}. The decay of Tri becomes faster (or slower) by increasing the rate constant of OH addition (or H-abstraction), respectively. This is mainly because of the OH addition regenerates the CI via R13, which further propagates radical chain oxidation.

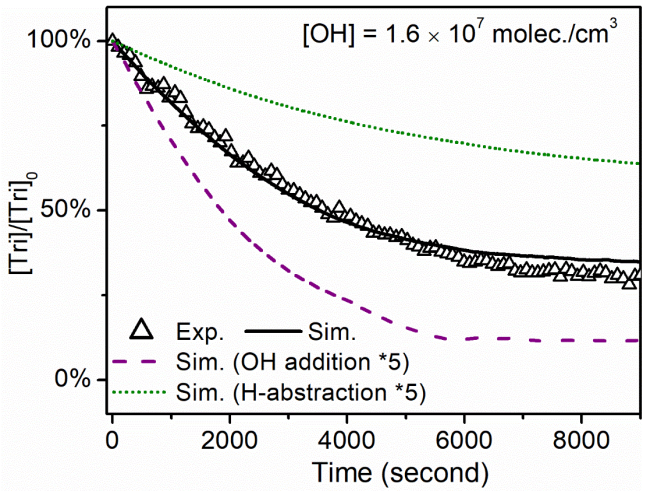

Figure S12. Sensitivity test of H-abstraction and OH addition rate coefficients. Symbols and lines are experimental and simulated results, respectively.

S2.4. Simulation results for Tri + O_3 reactions in the flow reactor

The kinetic model is compared with the Tri + O_3 experiments in the flow reactor. Figure S13 shows the simulated and experimental kinetics of Tri and TriO as a function of O_3 exposure (i.e. [O_3] × time). The model predictions are in reasonable agreement with experiments.

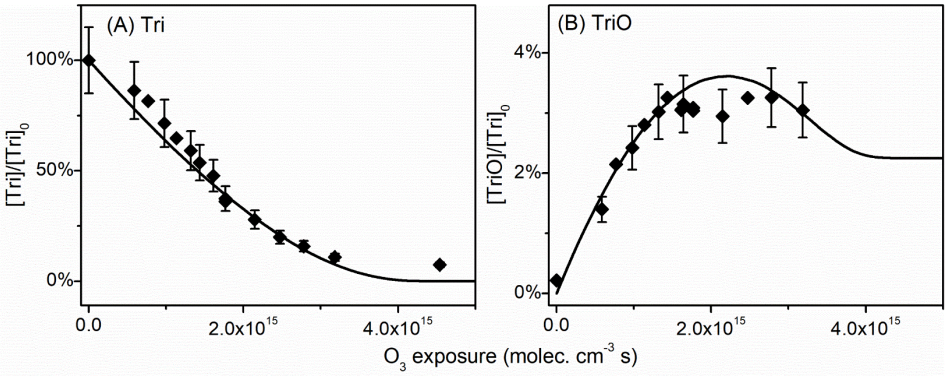

Figure S13. Experimental (symbols) and simulated (lines) normalized concentrations of Tri and TriO during Tri + O_3 reactions in the flow reactor (the average [O_3] ~ 4.0×10^{13} molecules·cm^{-3}).

A similar test, as was presented above for the Tri + OH reactions in Fig. S12, was conducted to examine the model sensitivity to the rate constants for OH addition and H-abstraction. As shown in Fig. S14, the decay of Tri becomes slower by increasing the rate constant for H-abstraction reaction. This is consistent with H-abstraction pathways leading to chain terminating products, whereas OH addition propagates further oxidation through the CI. Overall, the sensitivity tests show in Figs. S12 and S14 suggest that the SAR values in the model provide a reasonable description of the free radical sub-mechanism.

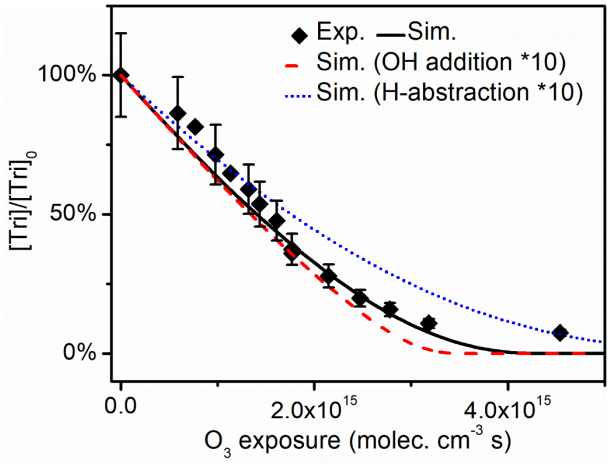

Figure S14. Sensitivity test of H-abstraction and OH addition rate coefficients. Symbols and lines are experimental and simulated results, respectively.

REFERENCES

(1) Che, D. L.; Smith, J. D.; Leone, S. R.; Ahmed, M.; Wilson, K. R. Quantifying the reactive uptake of OH by organic aerosols in a continuous flow stirred tank reactor. *Phys. Chem. Chem. Phys.* **2009**, 11, 7885-7895.

(2) Zeng, M.; Heine, N.; Wilson, K. R. Evidence that Criegee intermediates drive autoxidation in unsaturated lipids. *Proc. Natl. Acad. Sci. U.S.A.* **2020**, 117, 4486-4490.

(3) Heine, N.; Houle, F. A.; Wilson, K. R. Connecting the elementary reaction pathways of Criegee intermediates to the chemical erosion of squalene interfaces during ozonolysis. *Environ. Sci. Technol.* **2017**, 51, 13740-13748.

(4) Smith, J. D.; Kroll, J. H.; Cappa, C. D.; Che, D. L.; Liu, C. L.; Ahmed, M.; Leone, S. R.; Worsnop, D. R.; Wilson, K. R. The heterogeneous reaction of hydroxyl radicals with sub-micron squalane particles: a model system for understanding the oxidative aging of ambient aerosols. *Atmos. Chem. Phys. Discuss.* **2009**, 9, 3945-3981.

(5) Wilson, K. R.; Jimenez-Cruz, M.; Nicolas, C.; Belau, L.; Leone, S. R.; Ahmed, M. Thermal vaporization of biological nanoparticles: fragment-free vacuum ultraviolet photoionization mass spectra of tryptophan, phenylalanine-glycine-glycine, and β-carotene. *J. Phys. Chem. A* **2006**, 110, 2106-2113.

(6) Liu, C. L.; Smith, J. D.; Che, D. L.; Ahmed, M.; Leone, S. R.; Wilson, K. R. The direct observation of secondary radical chain chemistry in the heterogeneous reaction of chlorine atoms with submicron squalane droplets. *Phys. Chem. Chem. Phys.* **2011**, 13, 8993-9007.

(7) Hasson, A. S.; Chung, M. Y.; Kuwata, K. T.; Converse, A. D.; Krohn, D.; Paulson, S. E. Reaction of Criegee intermediates with water vapors - an additional source of OH radicals in alkene ozonolysis? *J. Phys. Chem. A* **2003**, 107, 6176-6182.

(8) Kumar, M.; Busch, D. H.; Subramaniam, B.; Thompson, W. H. Role of tunable acid catalysis in decomposition of α-hydroxyalkyl hydroperoxides and mechanistic implications for tropospheric chemistry. *J. Phys. Chem. A* **2014**, 118, 9701-9711.

(9) Hinsberg, W.; Houle, F., Kinetiscope: a stochastic kinetics simulator, Version 1.1.956, 2020, http://hinsberg.net/kinetiscope/.

(10) Houle, F. A.; Hinsberg, W. D.; Wilson, K. R. Oxidation of a model alkane aerosol by OH radical: the emergent nature of reactive uptake. *Phys. Chem. Chem. Phys.* **2015**, 17, 4412-4423.

(11) Houle, F. A.; Wiegel, A. A.; Wilson, K. R. Changes in reactivity as chemistry becomes confined to an interface. The case of free radical oxidation of $C_{30}H_{62}$ alkane by OH. *J. Phys. Chem. Lett.* **2018**, 9, 1053-1057.

(12) Houle, F. A.; Wiegel, A. A.; Wilson, K. R. Predicting aerosol reactivity across scales: from the laboratory to the atmosphere. *Environ. Sci. Technol.* **2018**, 52, 13774−13781.

(13) Wiegel, A. A.; Wilson, K. R.; Hinsberg, W. D.; Houle, F. A. Stochastic methods for aerosol chemistry: a compact molecular description of functionalization and fragmentation in the heterogeneous oxidation of squalane aerosol by OH radicals. *Phys. Chem. Chem. Phys.* **2015**, 17, 4398-4411.

(14) Heine, N.; Arata, C.; Goldstein, A. H.; Houle, F. A.; Wilson, K. R. Multiphase mechanism for the production of sulfuric acid from SO_2 by Criegee intermediates formed during the heterogeneous reaction of ozone with squalene. *J. Phys. Chem. Lett.* **2018**, 9, 3504-3510.

(15) Richards-Henderson, N. K.; Goldstein, A. H.; Wilson, K. R. Large enhancement in the heterogeneous oxidation rate of organic aerosols by hydroxyl radicals in the presence of nitric oxide. *J. Phys. Chem. Lett.* **2015**, 6, 4451-4455.

(16) Richards-Henderson, N. K.; Goldstein, A. H.; Wilson, K. R. Sulfur dioxide accelerates the heterogeneous oxidation rate of organic aerosol by hydroxyl radicals. *Environ. Sci. Technol.* **2016**, 50, 3554-3561.
(17) Li, M.; Su, H.; Li, G.; Ma, N.; Pöschl, U.; Cheng, Y. Relative importance of gas uptake on aerosol and ground surfaces characterized by equivalent uptake coefficients. *Atmos. Chem. Phys.* **2019**, 19, 10981-11011.
(18) Stephens, S.; Rossi, M. J.; Golden, D. M. The Heterogeneous Reaction of Ozone on Carbonaceous Surfaces. *Int. J. Chem. Kinet.* **1986**, 18, 1133-1149.
(19) Zhou, S.; Forbes, M. W.; Abbatt, J. P. Kinetics and products from heterogeneous oxidation of squalene with ozone. *Environ. Sci. Technol.* **2016**, 50, 11688-11697.
(20) Zhou, Z.; Zhou, S.; Abbatt, J. P. D. Kinetics and condensed-phase products in multiphase ozonolysis of an unsaturated triglyceride. *Environ. Sci. Technol.* **2019**, 53, 12467-12475.
(21) Zhang, X.; Barraza, K. M.; Beauchamp, J. L. Cholesterol provides nonsacrificial protection of membrane lipids from chemical damage at air-water interface. *Proc. Natl. Acad. Sci. U.S.A.* **2018**, 27, 3255-3260.
(22) Zhang, X.; Barraza, K. M.; Upton, K. T.; Beauchamp, J. L. Subtle changes in lipid environment have profound effects on membrane oxidation chemistry. *J. Am. Chem. Soc.* **2018**, 140, 17492-17498.
(23) Vereecken, L.; Novelli, A.; Taraborrelli, D. Unimolecular decay strongly limits the atmospheric impact of Criegee intermediates. *Phys. Chem. Chem. Phys.* **2017**, 19, 31599-31612.
(24) Peeters, J.; Boullart, W.; Pultau, V.; Vandenberk, S.; Vereecken, L. Structure-activity relationship for the addition of OH to (poly)alkenes: site-specific and total rate constants. *J. Phys. Chem. A* **2007**, 111, 1618-1631.
(25) Denisov, E. T.; Afanas'ev, I. B., *Oxidation and Antioxidants in Organic Chemistry and Biology*. Taylor & Frances: Oxford, 2005.
(26) Vereecken, L.; Peeters, J. H-atom abstraction by OH-radicals from (biogenic) (poly)alkenes: C±H bond strengths and abstraction rates. *Chem. Phys. Lett.* **2001**, 333, 162-168.
(27) Atkinson, R. Estimations of OH radical rate constants from H-atom abstraction from C-H and O-H bonds over the temperature range 250-1000 K. *Int. J Chem. Kinet.* **1986**, 18, 555-568.
(28) Buras, Z. J.; Elsamra, R. M.; Jalan, A.; Middaugh, J. E.; Green, W. H. Direct kinetic measurements of reactions between the simplest Criegee intermediate CH_2OO and alkenes. *J. Phys. Chem. A* **2014**, 118, 1997-2006.
(29) Tsang, W. Chemical Kinetic Data Base for Combustion Chemistry Part V. Propene. *J. Phys. Chem. Ref. Data* **1991**, 20, 221-273.
(30) Villano, S. M.; Huynh, L. K.; Carstensen, H. H.; Dean, A. M. High-pressure rate rules for alkyl + O_2 reactions. 1. The dissociation, concerted elimination, and isomerization channels of the alkyl peroxy radical. *J. Phys. Chem. A* **2011**, 115, 13425-13442.
(31) Zádor, J.; Miller, J. A. Adventures on the C_3H_5O potential energy surface: OH + propyne, OH + allene and related reactions. *Proc. Combust. Inst.* **2015**, 35, 181-188.
(32) Curran, H. J. Rate constant estimation for C_1 to C_4 alkyl and alkoxyl radical decomposition. *Int. J. Chem. Kinet.* **2006**, 38, 250-275.
(33) Vereecken, L.; Harder, H.; Novelli, A. The reactions of Criegee intermediates with alkenes, ozone, and carbonyl oxides. *Phys. Chem. Chem. Phys.* **2014**, 16, 4039-4049.
(34) Petrick, L.; Dubowski, Y. Heterogeneous oxidation of squalene film by ozone under various indoor conditions. *Indoor Air* **2009**, 19, 381-391.

(35) Wells, J. R.; Morrison, G. C.; Coleman, B. K. Kinetics and Reaction Products of Ozone and Surface-Bound Squalene. *J. ASTM Int.* **2008**, 5, 1-12.
(36) Zhou, S.; Joudan, S.; Forbes, M. W.; Zhou, Z.; Abbatt, J. P. D. Reaction of condensed-phase Criegee intermediates with carboxylic acids and perfluoroalkyl carboxylic acids. *Environ. Sci. Technol. Lett.* **2019**, 6, 243-250.
(37) Carstensen, H.-H.; Dean, A. M. Rate constants for the abstraction reactions RO_2 + C_2H_6; R = H, CH_3, and C_2H_5. *Proc. Combust. Inst.* **2005**, 30, 995-1003.
(38) Carstensen, H.-H.; Dean, A. M.; Deutschmann, O. Rate constants for the H abstraction from alkanes (R–H) by R'O_2 radicals: A systematic study on the impact of R and R'. *Proc. Combust. Inst.* **2007**, 31, 149-157.
(39) Zádor, J.; Taatjes, C. A.; Fernandes, R. X. Kinetics of elementary reactions in low-temperature autoignition chemistry. *Prog. Energy Combust. Sci.* **2011**, 37, 371-421.